

A comparative study of the magnetic properties of bulk and nanocrystalline Co_3O_4

This article has been downloaded from IOPscience. Please scroll down to see the full text article.

2008 J. Phys.: Condens. Matter 20 015218

(<http://iopscience.iop.org/0953-8984/20/1/015218>)

View [the table of contents for this issue](#), or go to the [journal homepage](#) for more

Download details:

IP Address: 193.2.92.59

The article was downloaded on 22/10/2012 at 06:59

Please note that [terms and conditions apply](#).

A comparative study of the magnetic properties of bulk and nanocrystalline Co_3O_4

P Dutta¹, M S Seehra^{1,3}, S Thota² and J Kumar²

¹ Department of Physics, West Virginia University, Morgantown, WV 26506-6315, USA

² Materials Science Programme, Indian Institute of Technology Kanpur, Kanpur 208016, India

E-mail: mseehra@wvu.edu

Received 14 September 2007, in final form 31 October 2007

Published 7 December 2007

Online at stacks.iop.org/JPhysCM/20/015218

Abstract

A comparative study of the magnetic and electron paramagnetic resonance (EPR) parameters of bulk and Co_3O_4 nanoparticles (NP), synthesized by a sol–gel process, is presented. Both samples possess the cubic phase with a slightly lower (by 0.34%) lattice parameter for the Co_3O_4 NP. The average crystallite size $D = 17$ nm determined by x-ray diffraction (XRD) for the Co_3O_4 NP is quite consistent with the electron microscopic observations. The bulk Co_3O_4 has particle size in the 1–2 μm range. A Néel temperature of $T_N = 30$ K (lower than the 40 K usually quoted in the literature) is determined from the analysis of the magnetic susceptibility versus temperature data for bulk Co_3O_4 . This $T_N = 30$ K is in excellent agreement with the $T_N = 29.92$ K reported from specific heat measurements. The Co_3O_4 NP powder exhibits a still lower $T_N = 26$ K, possibly due to the associated finite size effects. The values of coercivity, $H_c = 250$ Oe, and exchange bias, $H_e = -350$ Oe, together with the training effect have been observed in the Co_3O_4 NP sample (cooled in 20 kOe). Both H_c and H_e approach zero as $T \rightarrow T_N^-$. For $T > T_N$, the χ versus T data for both samples fit the modified Curie–Weiss law ($\chi = \chi_0 + C/(T + \theta)$). The magnitudes of C , θ and T_N are used to determine the following: exchange constants $J_{1\text{ex}} = 11.7$ K, $J_{2\text{ex}} = 2.3$ K, and magnetic moment per Co^{2+} ion $\mu = 4.27 \mu_B$ for bulk Co_3O_4 ; and $J_{1\text{ex}} = 11.5$ K, $J_{2\text{ex}} = 2.3$ K and $\mu = 4.09 \mu_B$ for Co_3O_4 NP. EPR yields a single Lorentzian line near $g = 2.18$ in both samples but with a linewidth ΔH that is larger for the Co_3O_4 NP. Details of the temperature dependence of ΔH , line intensity I_0 , and disappearance of the EPR on approach to T_N are different for the two samples. These effects are discussed in terms of spin–phonon interaction and additional surface anisotropy present in Co_3O_4 NP.

1. Introduction

Nanocrystalline materials derive their interesting and technologically useful properties with respect to bulk mainly from quantum confinement effects and the increasing role of surface atoms with the decrease in particle size D [1, 2]. A comparison of the specific properties of nanoparticles (NP) and the corresponding bulk sample is therefore likely to provide new insights into the associated differences. Co_3O_4 is described by a formula unit AB_2O_4 ($\text{A} \rightarrow \text{Co}^{2+}$, $\text{B} \rightarrow \text{Co}^{3+}$) and exhibits a normal spinel crystal structure with occupation of tetrahedral

A sites by Co^{2+} and octahedral B sites by Co^{3+} . Its magnetic moment arises due to Co^{2+} ions largely because of spins, with a small contribution from spin–orbit coupling [3]. On the other hand, Co^{3+} ions have no permanent magnetic moment as a consequence of the splitting of 3d levels by the octahedral crystal field and complete filling of t_{2g} levels. Co_3O_4 behaves like an antiferromagnet (AF) with the Néel temperature $T_N \approx 40$ K with each Co^{2+} ion in the A-site having four neighboring Co^{2+} ions of opposite spins [3]. Two paths for the superexchange interaction between Co^{2+} ions have been suggested: A–O–A with $z_1 = 4$ neighbors and A–O–B–O–A with $z_2 = 12$ neighbors (O stands for the oxygen O^{2-} ion) but without

³ Author to whom any correspondence should be addressed.

specifying their relative strengths [3]. Angelov *et al* [4] reported a nearly linear temperature dependence of the electron paramagnetic resonance (EPR) linewidth ΔH in bulk Co_3O_4 , prepared by decomposition of $\text{Co}(\text{NO}_3)_2 \cdot 6\text{H}_2\text{O}$ at different temperatures (623–1073 K). Although the value of ΔH was found to decrease with increase in the decomposition temperature [4], an appropriate interpretation of these results was not provided [4]. Of course, no EPR line was observed below T_N , as is generally the case for anisotropic antiferromagnets [5, 6].

A number of studies have been reported recently for Co_3O_4 NP: (a) Takada *et al* [7] dispersed 3 nm Co_3O_4 particles in SiO_2 and reported a superparamagnetic behavior with a blocking temperature $T_B = 3.4$ K; (b) Li *et al* [8] studied Co_3O_4 NP of (i) size 14 nm and (ii) of size 12 nm but capped by polymer decomposition residues and reported an increase in coercivity (H_c) and exchange-bias (H_e) for the capped NP; (c) Makhlof [9] reported $T_B = 25$ K for Co_3O_4 NP of size ~ 20 nm and Curie–Weiss behavior of the magnetic susceptibility $\chi = C/(T + \theta)$ for $T > T_B$; (d) Salabas *et al* [10] prepared Co_3O_4 nanowires of diameter 8 nm and lengths up to 100 nm (by the nanocasting route) and observed blocking temperature $T_B = 30$ K and non-zero H_e for $T < T_B$.

In this work, a comparative study of the properties of bulk and nanocrystalline Co_3O_4 is reported in terms of magnetic parameters (namely Néel temperature, magnetic susceptibility χ , coercivity H_c and exchange bias H_e) under different conditions and the temperature-dependent behavior of the EPR parameters (i.e. linewidth ΔH , resonance field H_r and intensity I_0) on approach to T_N . Substantial differences observed between the bulk and nanocrystalline samples are interpreted in terms of finite size effects and the dominant role of surface atoms in NP. The exchange constants for the two samples are also determined.

2. Experimental details

The bulk Co_3O_4 powder obtained from Aldrich Chemicals was used as-received without any further modification. The nanocrystalline Co_3O_4 was synthesized by a sol–gel process using cobalt acetate tetrahydrate [$\text{Co}(\text{CH}_3\text{COO})_2 \cdot 4\text{H}_2\text{O}$] and oxalic acid as precursors and ethanol as solvent. For this, 2 g of cobalt acetate tetrahydrate was dissolved in about 200 ml of ethanol under constant stirring and heating at 45 °C for 30 min to obtain a light pink color sol. A solution of 6 g of oxalic acid solution in 200 ml of ethanol was then added to the above warm sol to yield a thick gel. This product was then dried at 80 °C for 24 h to produce pink flakes/powder of cobalt oxalate hydrate $\text{CoC}_2\text{O}_4 \cdot x\text{H}_2\text{O}$. Thermogravimetric analysis (TGA) indicated complete decomposition of cobalt oxalate hydrate to Co_3O_4 at temperatures above 400 °C. The product was therefore calcined at 500 °C for 2 h in air for further study. An x-ray powder diffractometer (Rigaku Model D/Max) with Cu $K\alpha$ radiation ($\lambda = 1.54185$ Å) was used for phase evaluation, and scanning and transmission electron microscopes (FEI Quanta 200 HV and FEI Tecnai 20 G2, respectively) were used for morphology. A commercial superconducting quantum interference device (SQUID) magnetometer with temperature capabilities of 2–380 K and magnetic field (H) up to ± 70 kOe

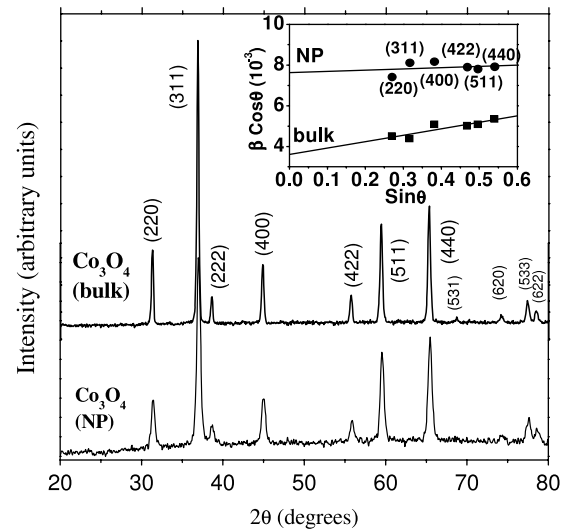


Figure 1. X-ray diffraction patterns of the bulk and Co_3O_4 NP with Miller indices of the peaks marked. The inset shows $\beta \cos \theta$ versus $\sin \theta$ plots, whose fit to $\beta \cos \theta = (0.89\lambda/D) + \eta \sin \theta$, yields particle size $D = 17 \pm 3$ nm and strain $\eta = 6.3 \times 10^{-4}$ for Co_3O_4 NP and $D = 40 \pm 5$ nm and $\eta = 3.4 \times 10^{-3}$ for bulk Co_3O_4 .

was employed for measurements of the magnetization (M). EPR measurements were made with a standard reflection-type spectrometer operating at 9.28 GHz in conjunction with a variable temperature cryostat (4.2–300 K).

3. Results and discussion

3.1. Phase evaluation and morphology

Figure 1 shows x-ray diffraction (XRD) patterns of both bulk and nanocrystalline Co_3O_4 samples. These correspond to the cubic phase of Co_3O_4 and space group $Fd3m$ [11] with lattice constants $a = 8.09 \pm 0.02$ Å for bulk Co_3O_4 and $a = 8.06 \pm 0.02$ Å for Co_3O_4 NP. The average crystallite size D and strain η are determined by making a Williamson–Hall ($\beta \cos \theta$ versus $\sin \theta$) plot (the relation being $\beta \cos \theta = (0.89\lambda/D) + \eta \sin \theta$), using the values for the diffraction peak width (β) obtained after correction for instrumental broadening [12, 13]. The values of D and η as deduced are given in the caption to figure 1. The XRD crystallite size of the Co_3O_4 NP prepared by the sol–gel process is ~ 17 nm. A typical scanning electron micrograph (figure 2(a)) recorded in secondary electron (SE) mode reveals the presence of nanorods (average diameter ~ 100 nm and aspect ratio 20) each stacked like a bamboo stick. Also, each nanorod consists of a large number of tiny spherical particles. Figure 2(b) shows a bright field (BF) transmission electron micrograph of nanocrystalline Co_3O_4 powder observed at 200 keV. It shows particles in the size range 15–20 nm in agreement with the size determined from XRD. The corresponding selected area diffraction (SAD) pattern given in figure 2(c) matches well with the cubic phase of Co_3O_4 described above. For the bulk sample, the scanning electron micrograph shows particles of 1–2 μm (figure 3), much larger than the size of 40 nm determined by XRD in figure 1. However, for $D > 30$ nm, sizes determined by

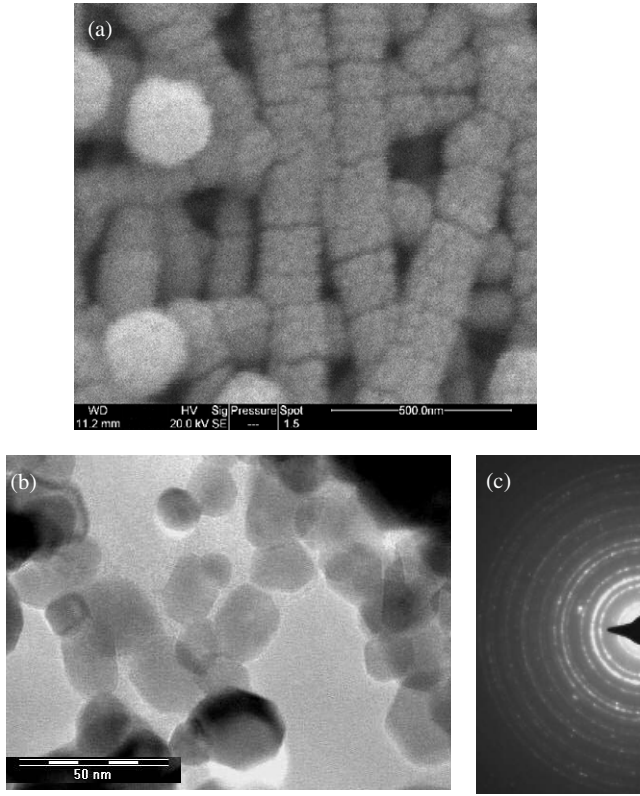


Figure 2. (a) Scanning electron micrograph of Co₃O₄ NP showing nanorods of bamboo morphology with diameters $\simeq 100$ nm and comprising many tiny particles of size about 20 nm. (b) TEM bright field image depicting particles in the size range 15–20 nm. (c) Electron diffraction pattern corresponding to (b) matching well with the cubic phase of Co₃O₄.

XRD line broadening are not reliable because the instrument corrected β is too small, yielding large errors in size D .

3.2. Temperature dependence of magnetic susceptibility

The magnetic susceptibility (χ) versus temperature plots for the bulk and nanocrystalline Co₃O₄ samples are shown in figure 4. For the zero-field-cooled (ZFC) case, the sample was cooled from 300 to 2 K and then a magnetic field $H = 500$ Oe was turned on for magnetization (M) measurements with increasing temperature after ensuring stabilization at each temperature. Upon reaching 370 K, the data were similarly collected with decreasing temperature (FC mode) keeping the same applied field. The susceptibility (χ) versus temperature plots exhibit peaks at 38 and 35 K for the bulk and Co₃O₄ NP, respectively. A clear bifurcation of the FC and ZFC plots, observed only for the NP case near 29 K, is a typical signature of superparamagnetic blocking in magnetic NP. Interestingly, the bifurcation occurs at a temperature (i.e. $T_{\text{irr}} = 29$ K) lower than T_p (35 K). Also, flattening of χ versus T plots at low temperatures (below T_{irr}) is indicative of significant interaction among the NP [2]. For the bulk Co₃O₄, the χ versus T plot is characteristic of an antiferromagnet such as CoO in that χ becomes temperature-independent at the lower temperatures because the contribution from the orbital moment is partially

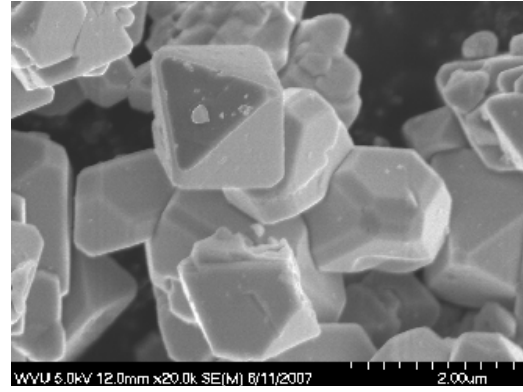


Figure 3. Scanning electron micrograph of bulk Co₃O₄ showing particles with sizes 1–2 μm .

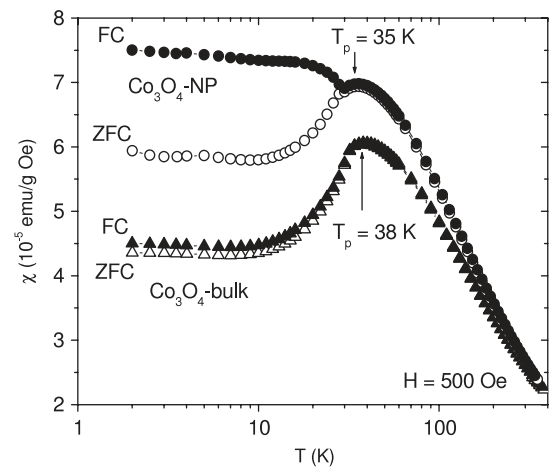


Figure 4. Temperature dependence of the magnetic susceptibility (χ) for bulk and Co₃O₄ NP under the zero-field-cooled (ZFC) and field-cooled (FC) conditions. T_p denotes the peak position in χ versus T plots. Note the bifurcation of χ_{ZFC} and χ_{FC} curves of Co₃O₄ NP below ~ 29 K.

restored by the spin–orbit coupling [14, 15]. For the Co₃O₄ NP, the magnitude of χ is somewhat larger at all T as compared to bulk Co₃O₄, suggesting an additional contribution to χ , perhaps due to uncompensated surface spins.

It is well known that the peak in the magnetic susceptibility in antiferromagnets usually occurs at a temperature few per cent higher than T_N ; instead, T_N is defined by the peak in the $\partial(\chi T)/\partial T$ versus T plot [16, 17]. The $(\chi_p T)$ versus T and $\partial(\chi_p T)/\partial T$ versus T plots for the two samples (bulk and NP) are shown in figure 5, where $\chi_p = (\chi - \chi_0)$ is the paramagnetic susceptibility of a polycrystalline sample corrected for the temperature-independent contribution $\chi_0 = 3.06 \times 10^{-6}$ emu g⁻¹ Oe⁻¹ of Co₃O₄ discussed later. These plots yield $T_N = 30$ and 26 K for bulk and Co₃O₄ NP, respectively. The value of $T_N = 30$ K for bulk Co₃O₄ is lower than the $T_N \simeq 40$ K often quoted for Co₃O₄ [3, 4]. However, measurements of the specific heat C_p for bulk Co₃O₄ in the temperature range 5–307 K indicate a peak in C_p corresponding to $T_N = (29.92 \pm 0.03)$ K [18]. Thus, $T_N = 30$ K

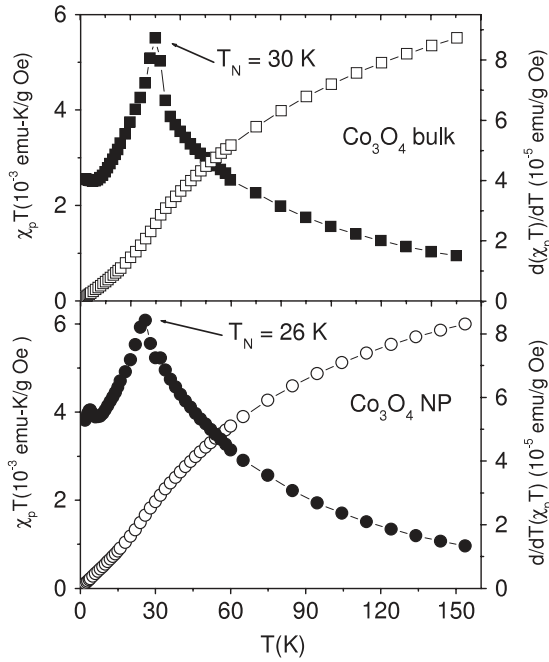


Figure 5. Plots of $(\chi_p T)$ versus T and $d(\chi_p T)/dT$ versus T plots for the bulk and Co_3O_4 NP where $\chi_p = \chi - \chi_0$ with $\chi_0 = 3.06 \times 10^{-6} \text{ emu g}^{-1} \text{ Oe}^{-1}$ (see text). The peak in the $d(\chi_p T)/dT$ versus T plot defines the Néel temperature T_N . Note the lower value of T_N for the Co_3O_4 NP sample.

determined from two independent techniques (i.e. χ_p and C_p measurements) is the characteristic value for bulk Co_3O_4 . The decrease of T_N to 26 K for the Co_3O_4 NP can be understood on the basis of the finite size effects (decrease in particle size D) [19, 20]. Resnick *et al* [21] have reported $T_N = 15 \pm 2 \text{ K}$ in Co_3O_4 NP of still smaller size of 4 nm in line with the expected decrease of T_N with decrease in size D .

Some additional features of the data in figures 4 and 5 deserve further discussion. First χ for bulk Co_3O_4 in figure 4 becomes essentially temperature-independent for $T < 10 \text{ K}$. This is similar to other Co^{2+} antiferromagnets such as CoO [15] and CoF_2 [22] in which the orbital contribution to the magnetic moment of Co^{2+} has been shown to result in non-zero easy-axis or parallel susceptibility χ_{11} in the limit of $T \rightarrow 0 \text{ K}$. This also leads to temperature-independent χ_{11} and hence χ_p at lower temperatures. A similar effect is probably present in Co_3O_4 . The weak anomalies in the plots of $\partial(\chi_p T)/\partial T$ observed in figure 5 near 10 K are simply related to this change in the slope of χ_p versus T data near 10 K in figure 4.

For $T > T_p$, the data of χ versus T of figure 4 are fitted to the modified Curie–Weiss law $\chi = \chi_0 + [C/(T + \theta)]$ with $C = N\mu^2/3k_B$, $\mu^2 = g^2 J(J+1) \mu_B^2$, θ the Curie–Weiss temperature and χ_0 contains the temperature-independent orbital contribution mentioned earlier and the diamagnetic contribution of $\chi_d = -3.3 \times 10^{-7} \text{ emu g}^{-1} \text{ Oe}^{-1}$ [23]. Usually χ_0 is estimated from the plot of χ versus $1/T$ in the limit of $1/T \rightarrow 0$ using the high temperature data. In [3], $\chi_0 = 3.06 \times 10^{-6} \text{ emu g}^{-1} \text{ Oe}^{-1}$ was estimated for bulk Co_3O_4 using the χ versus T data up to 1000 K. A similar procedure for our data up to 380 K in figure 4 yields $\chi_0 =$

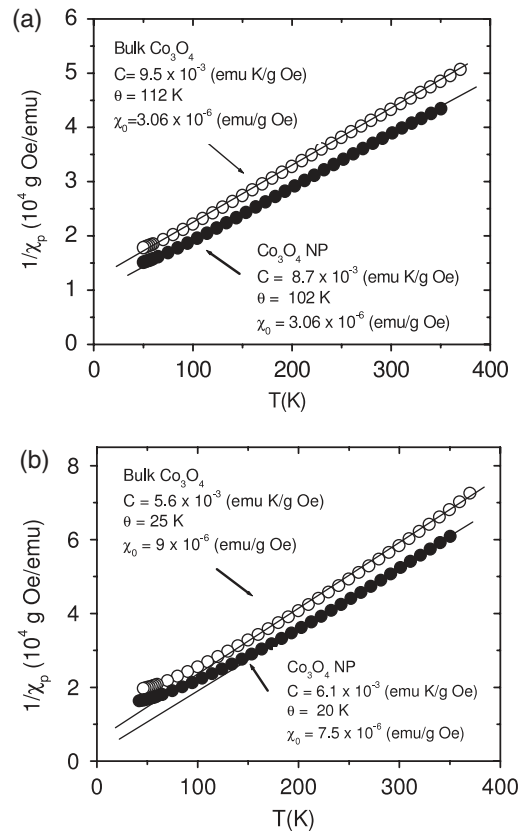


Figure 6. (a) $1/\chi_p$ versus T plot for the bulk and Co_3O_4 NP with $\chi_0 = 3.06 \times 10^{-6} \text{ emu g}^{-1} \text{ Oe}^{-1}$. The solid lines represent linear fit to the Curie–Weiss law: $\chi_p = C/(T + \theta)$. (b) The same except for different χ_0 listed in the figure and discussed in the text.

9×10^{-6} (7.5×10^{-6}) $\text{emu g}^{-1} \text{ Oe}^{-1}$ for the bulk (NP) Co_3O_4 . We argue later that $\chi_0 = 3.06 \times 10^{-6} \text{ emu g}^{-1} \text{ Oe}^{-1}$ is a more reliable estimate, partly because extrapolation of the limit of $1/T \rightarrow 0$ is expected to be more accurate near 1000 K than near 380 K. The plots of $1/\chi_p$ versus T are shown in figures 6(a) and (b) using the two sets of the magnitudes discussed above. The magnitudes of C and θ determined from these fits to the modified Curie–Weiss law are listed in the figures. It is evident that the plots of figure 6(a) using $\chi_0 = 3.06 \times 10^{-6} \text{ emu g}^{-1} \text{ Oe}^{-1}$ yield the expected linear variation over a wider temperature range, pointing to greater reliability of these fits. For these reasons, we have used the magnitudes of C and θ listed in figure 6(a) to estimate the exchange constants for Co_3O_4 .

3.3. Exchange constants

As mentioned in section 1, there are two possible paths for superexchange interaction between Co^{2+} ions: A–O–A and A–O–B–O–A with $z_1 = 4$ and $z_2 = 12$, respectively. If the corresponding exchange constants are represented by $J_{1\text{ex}}$ and $J_{2\text{ex}}$, the expression for T_N and θ , using the molecular field theory [24], can be written as:

$$T_N = \frac{J(J+1)}{3k_B} (J_{1\text{ex}} z_1 - J_{2\text{ex}} z_2) \quad (1)$$

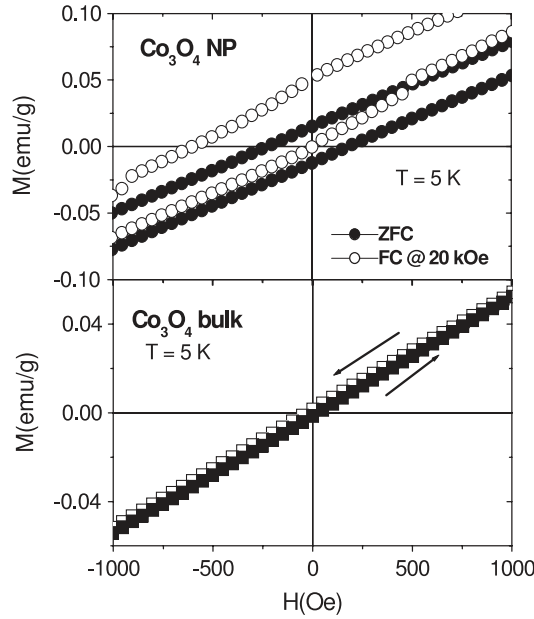


Figure 7. Hysteresis loops of bulk and Co_3O_4 NP recorded at 5 K in the lower field region of ± 1 kOe. The minute irreversibility observed for the direct and reverse field scans for bulk Co_3O_4 is within the experimental uncertainty of the SQUID magnetometer. A shifted hysteresis loop with enhanced coercivity can be clearly noticed for the Co_3O_4 NP field cooled (FC) in $H = 20$ kOe.

$$\theta = \frac{J(J+1)}{3k_B} (J_{1\text{ex}}z_1 + J_{2\text{ex}}z_2). \quad (2)$$

To determine $J_{1\text{ex}}$ and $J_{2\text{ex}}$, the magnitude of effective $J(J+1)$ for Co^{2+} is needed. The Curie constant $C = N\mu^2/3k_B$ with $\mu^2 = g^2J(J+1)\mu_B^2$, g being the Landé factor and J the total angular momentum. Using the magnitudes of $g = 2$ and C as given in figure 6(a) one finds $\mu = 4.27 \mu_B$ for bulk Co_3O_4 and $\mu = 4.09 \mu_B$ for the Co_3O_4 NP. The spin contribution to the above magnitudes of μ is $3.87 \mu_B$ for Co^{2+} with spin $S = 3/2$. Obviously, there is some additional contribution resulting from the partially restored orbital angular momentum for the $^4F_{9/2}$ ground state of Co^{2+} [24]. Using equations (1) and (2) and the values of θ , T_N and μ for the two cases yields $J_{1\text{ex}} = 11.7$ K and $J_{2\text{ex}} = 2.3$ K for bulk, and $J_{1\text{ex}} = 11.5$ K and $J_{2\text{ex}} = 2.3$ K for Co_3O_4 NP. Thus, both the exchange constants $J_{1\text{ex}}$ and $J_{2\text{ex}}$ correspond to antiferromagnetic coupling. From the magnitudes of C in figure 6(b), $\mu = 3.28 \mu_B$ ($3.43 \mu_B$) is obtained for bulk(NP) Co_3O_4 . We consider these magnitudes of μ to be unphysical for Co^{2+} since they are even lower than the spin-only value of $\mu = 3.87 \mu_B$. Consequently the magnitudes of θ in figure 6(b) are also considered to be incorrect. Of course, the use of the molecular field theory to determine exchange constants has its own limitations since higher-order spin correlations are neglected in this model.

3.4. Coercivity and exchange bias

For a bulk antiferromagnet below T_N , magnetization is expected to vary linearly with applied field H below the spin-flop field, with zero H_c and H_e . This indeed is observed in bulk Co_3O_4 (figure 7). However, for the Co_3O_4 NP, the data at 5 K

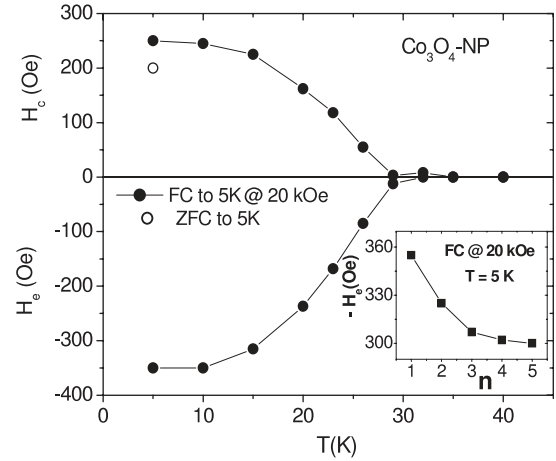


Figure 8. Temperature dependence of coercivity (H_c) and exchange-bias (H_e) for the Co_3O_4 NP in the 5–40 K FC case at 20 kOe and at 5 K under ZFC conditions. Note the zero values of H_c and H_e above T_N . The inset shows the progressive decrease of the magnitude of exchange-bias (H_e) after successive scans denoted by n at 5 K. The lines joining the data points are a visual aid.

show a symmetric hysteresis loop with $H_c = 200$ Oe for the ZFC sample and a shifted hysteresis loop with $H_c = 250$ Oe and $H_e = -350$ Oe for the sample cooled in $H = 20$ kOe from 300 to 5 K (figure 8). Thus, cooling the sample in a magnetic field produces an exchange-bias and leads to enhancement of H_c as well.

The temperature dependence of H_c and H_e for the Co_3O_4 NP cooled under $H = 20$ kOe from 300 K to the measuring temperature is shown in figure 8. Both H_c and H_e become zero above T_N . The inset to figure 8 depicts the training effect, namely change in H_e for the sample cycled through several successive hysteresis loops (designated by ' n ' at 5 K). A similar effect was reported recently by Salabas *et al* [10] in Co_3O_4 nanowires of 8 nm diameter, although the magnitudes of H_e and H_c in their case are somewhat smaller.

The existence of the exchange-bias H_e suggests the presence of a ferromagnetic/antiferromagnetic (F/AF) interface with F-like surface spins covering the core of the antiferromagnetically ordered spins in Co_3O_4 NP. Furthermore, the observation of the training effect and open loops up to 55 kOe suggests the surface spins to be in an unstable spin-glass-like state [10]. Such a spin-glass ordering results from the weaker exchange-coupling experienced by the surface spins due to reduced coordination at the surface. These effects, however, disappear above T_N when the spins in the core become disordered. The observation of a somewhat lower magnetic moment per Co^{2+} ion, smaller values of exchange constant $J_{1\text{ex}}$ and lower T_N observed for the Co_3O_4 NP compared with bulk Co_3O_4 may all be due to the weak exchange coupling and reduced coordination of the surface spins.

3.5. Temperature dependence of paramagnetic resonance

For both the NP and bulk Co_3O_4 samples, EPR spectra were recorded from 300 K down to T_N (below which the EPR line disappears) at 9.282 GHz. At all temperatures, only a

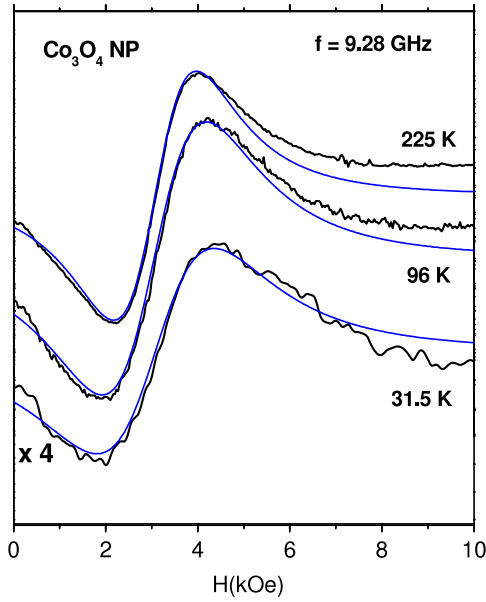


Figure 9. The standard derivative EPR spectra at several representative temperatures. The smooth solid lines are Lorentzian fits.

(This figure is in colour only in the electronic version)

single line near $g = 2.19$ is observed for both bulk and NP Co_3O_4 . In figure 9, we show representative line spectra at three temperatures (225, 96 and 31.5 K) and their fits to the Lorentzian lineshape for NP Co_3O_4 . The fits are good except for some departures at the higher H well above the resonance field H_r . In addition to H_r , the linewidth ΔH (peak-to-peak separation in the absorption derivative) and the line intensity $I_0 = \alpha (\Delta H)^2 \ell$ were measured where ℓ is the peak-to-peak height and $\alpha = 3.63$ (1.033) for the Lorentzian (Gaussian) lineshape. Since the lineshape is essentially unchanged with temperature, $(\Delta H)^2 \ell$ provides a good measure of relative change in I_0 with T . In figure 10, the temperature dependences of H_r , ΔH and I_0 are plotted for both bulk and NP Co_3O_4 . The following observations are noteworthy:

- All the EPR parameters namely, ΔH , H_r and I_0 , have higher values for the Co_3O_4 NP.
- The line intensity I_0 decreases rapidly whereas ΔH increases on approach to T_N for both samples so that resonance is not observed at T_N as expected and as observed in other anisotropic antiferromagnets [5].
- For the Co_3O_4 NP, the line intensity I_0 peaks near 75 K and ΔH reaches a minimum value near 100 K, signaling the onset of short range magnetic ordering. For the bulk Co_3O_4 similar changes in I_0 are observed below 150 K with only a change in the slope of ΔH versus T variation.
- For bulk Co_3O_4 , there is some temperature dependence of H_r above 150 K. This is the paramagnetic region since intensity I_0 decreases with increase in temperature. This change in g -value is not yet understood.
- Significantly larger values of ΔH observed at all temperatures for the Co_3O_4 NP are related to size effects in NP. As discussed below, this finding is in agreement with

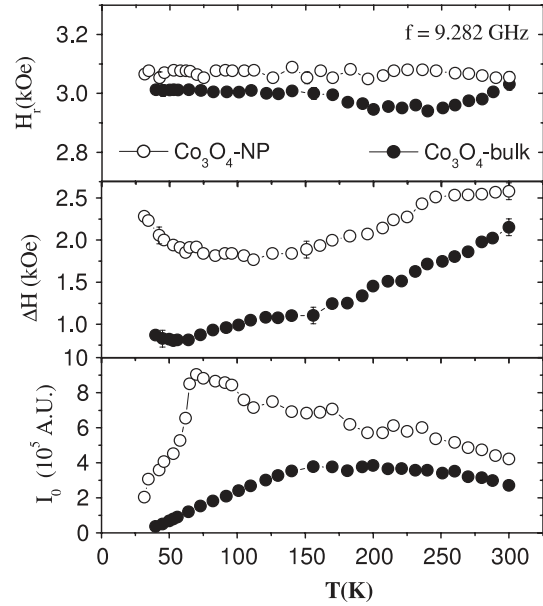


Figure 10. Temperature dependence of the EPR parameters, namely resonance field H_r , linewidth ΔH and intensity I_0 , for the bulk and Co_3O_4 NP.

the reported EPR studies of Angelov *et al* [4] on a number of Co_3O_4 samples prepared by the decomposition of $\text{Co}(\text{NO}_3)_2 \cdot 6\text{H}_2\text{O}$ at different temperatures (623–1073 K). In this work, the samples synthesized at a lower decomposition temperatures showed higher ΔH without affecting the g -value.

The average particle size D for the oxide NPs such as NiO and CuO is found to increase with increase in the annealing temperature during the preparation stage [25–27]. If a similar behavior is assumed for Co_3O_4 samples, the progressive increase in ΔH values observed by Angelov *et al* [4] with decrease in decomposition temperature can be attributed to a correspondingly smaller average particle size, although these authors did not measure the particle size of their samples. The observations of larger values of ΔH found in Co_3O_4 NP is thus a general phenomenon which can be qualitatively explained by the presence of enhanced anisotropy in NP as discussed below.

EPR linewidth ΔH is broadened by anisotropic spin interactions and narrowed by exchange interaction such that $\Delta H \sim H_a^2/H_{\text{ex}}$, where H_a and H_{ex} are the equivalent anisotropy and exchange fields, respectively [28, 29]. Also, the effective anisotropy constant K_{eff} for a spherical nanoparticle of diameter D is given by [30, 31]:

$$K_{\text{eff}} = K_b + (6/D)K_s \quad (3)$$

where K_b is the bulk anisotropy constant, K_s is the surface anisotropy constant, and $6/D$ stands for the surface area to volume ratio for spherical particles. According to equation (3), the anisotropy for a nanoparticle is invariably enhanced because of the additional contribution arising from its surface. The corresponding increase in H_a combined with a slight reduction in the effective exchange field H_{ex} (lower J_{lex}

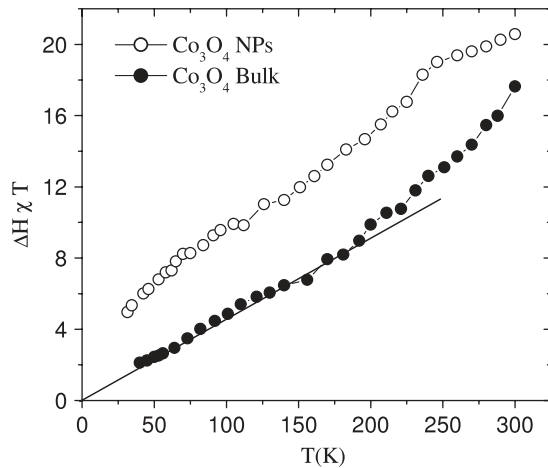


Figure 11. Temperature dependence of the product ($\Delta H \chi T$) for the bulk and Co_3O_4 NP. The solid line depicts linear variation at lower temperatures.

observed) should cause an increase in EPR linewidth for Co_3O_4 NP as observed in this work.

For systems with spin $S \geq 1$ and with some orbital contribution to their magnetic moment (such as Co^{2+} in Co_3O_4), spin–phonon interaction also contributes to ΔH [32, 33]. While the one-phonon process yields a contribution proportional to T and is applicable at lower temperatures, the two-phonon process shows T^2 dependence and dominates at higher temperatures. The linewidth ΔH at a temperature (T) for a polycrystalline sample in such cases is given by [32, 33]

$$\Delta H = \frac{C}{T\chi} \{K(T) + f(\varepsilon)\}, \quad (4)$$

where C is the Curie constant, $K(T)$ is the non-critical term arising because of spin–phonon interaction and $f(\varepsilon)$ is the critical contribution near T_N (with $\varepsilon = (T - T_N)/T_N$) resulting from magnetic short range ordering. Accordingly, the product ($\Delta H T \chi$) is expected to show temperature dependence in consonance with $K(T)$ and $f(\varepsilon)$. For CrBr_3 ferromagnet with $T_c = 32$ K, the product $\Delta H T \chi$ varies linearly with temperature for $T > 3T_c$ [32, 33] whereas for NiCl_2 , an antiferromagnet with $T_N = 49.5$ K, there is linear dependence at lower temperatures and T^2 dependence at higher temperatures [34]. In $\text{R}_{1-x}\text{B}_x\text{MnO}_{3+\delta}$ manganites ($\text{R} = \text{La}, \text{Pr}, \text{Br}, \text{Ca}, \text{Sr}$), data fitted to equation (4) indicated linear variation of $K(T)$ with temperature [35].

For the bulk and Co_3O_4 NP samples, the product $\Delta H T \chi$ versus T plots are shown in figure 11. There is evidence of T (T^2) dependence at the lower (higher) temperatures, signifying the role of spin–phonon interaction. The critical broadening of ΔH on approach to T_N represented by the $f(\varepsilon)$ term in equation (4) is more dominant for the Co_3O_4 NP than for bulk Co_3O_4 . Angelov *et al* [4] also reported more dominance of the $f(\varepsilon)$ term in those samples which were prepared at the lower decomposition temperatures (apparently having smaller particle size D). So, the short range magnetic order above T_N represented by $f(\varepsilon)$ is felt over a wider temperature range for the Co_3O_4 NP.

4. Concluding remarks

The analysis of the magnetic susceptibility data presented here for bulk Co_3O_4 has shown its Néel temperature $T_N = 30$ K to be significantly lower than the $T_N \simeq 40$ K usually quoted in literature. This value of T_N is in excellent agreement with $T_N = 29.92 \pm 0.03$ K determined from the heat capacity C_p versus T measurements [18]. A still lower $T_N = 26$ K observed for nanocrystalline Co_3O_4 is due to associated finite size effects. A comparison of the magnetic properties and EPR parameters presented here revealed: (a) the existence of coercivity and exchange bias due to weakly coupled surface spins in NP, (b) antiferromagnetic ordering of spins in the core below T_N , (c) higher anisotropy in NP and (d) the important role of the spin–phonon interaction. The exchange-constants reported here, based on the molecular field theory approximation and an extrapolated value of χ_0 , need to be verified by direct methods such as neutron diffraction [36]. The results presented here also suggest the need for additional studies on the particle size dependence of exchange-bias, T_N and EPR linewidth in Co_3O_4 NP. Such studies in well-characterized Co_3O_4 NP are planned for the near future. A theory for the temperature dependence of EPR parameters in antiferromagnetic NP is also needed along the lines of that for bulk antiferromagnets [5, 37].

Acknowledgments

Research at West Virginia University was supported in part by the US Department of Energy (contract no. DE-FC26-05NT42456).

References

- [1] See the review by Dormann J L, Fiorani D and Tronc E 1997 Magnetic relaxation in fine-particle systems *Advances in Chemical Physics* vol XCVIII, ed I Prigogine and S A Rice (New York: Wiley) p 283
- [2] Labarta A *et al* 2005 *Surface Effects in Magnetic Nanoparticles* ed D Fiorani (New York: Springer) p 109
- [3] Roth W L 1964 *J. Phys. Chem. Solids* **25** 1
- [4] Angelov S, Zhecheva E, Stoyanova R and Atanasov M 1990 *J. Phys. Chem. Solids* **51** 1157
- [5] See the review by Seehra M S and Huber D L 1975 *AIP Conf. Proc.* **24** 261
- [6] Seehra M S and Castner T G 1970 *Solid State Commun.* **8** 787
- [7] Takada S, Fujii M, Kohiki M, Babasaki T, Deguchi H, Mitome M and Oku M 2001 *Nano Lett.* **1** 379
- [8] Li S, Bi H, Cui B, Zhang F, Du Y, Jiang X, Yang C, Yu Q and Zhu Y 2004 *J. Appl. Phys.* **95** 7420
- [9] Makhlof S A 2002 *J. Magn. Magn. Mater.* **246** 184
- [10] Salabas E L, Rumblecker A, Kleitz F, Radu F and Schuth F 2006 *Nano Lett.* **6** 2977
- [11] JCPDS—International centre for diffraction data file 43-1003
- [12] Williamson G K and Hall W H 1953 *Acta Metall.* **1** 22
- [13] Dutta P, Manivannan A, Seehra M S, Shah N and Huffman G P 2004 *Phys. Rev. B* **70** 174428
- [14] Seehra M S and Silinsky P 1979 *Solid State Commun.* **31** 183
- [15] Silinsky P and Seehra M S 1981 *Phys. Rev. B* **24** 419
- [16] Fisher M E 1962 *Phil. Mag.* **7** 1731
- [17] Bragg E E and Seehra M S 1973 *Phys. Rev. B* **7** 4197
- [18] Khriplovich L M, Kholopov E V and Paukov I E 1982 *J. Chem. Thermodyn.* **14** 207
- [19] Ambrose T and Chien C L 1996 *Phys. Rev. Lett.* **76** 1743

- [20] Tang Y J, Smith D J, Zink B L, Hellman F and Berkowitz A E 2003 *Phys. Rev. B* **67** 054408
- [21] Resnick D A, Gilmore K, Idzerda Y U, Klem M T, Allen M, Douglas T, Arenholz E and Young M 2006 *J. Appl. Phys.* **99** 08Q501
- [22] Lines M E 1965 *Phys. Rev.* **137** A982
- [23] Nethravathi C, Sen S, Ravishankar N, Rajamathi M, Pietzonka C and Harbrecht B 2005 *J. Phys. Chem. B* **108** 11468
- [24] Morrish A H 2001 *The Physical Principles of Magnetism* (Piscataway, NJ: IEEE)
- [25] Makhlouf S A, Parker F T, Spada F E and Berkowitz A E 1997 *J. Appl. Phys.* **81** 5561
- [26] Seehra M S, Dutta P, Shim H and Manivannan A 2004 *Solid State Commun.* **129** 721
- [27] Punnoose A, Magnone H, Seehra M S and Bonevich J 2001 *Phys. Rev. B* **64** 174420
- [28] Castner T G and Seehra M S 1971 *Phys. Rev. B* **4** 38
- [29] Anderson P W and Weiss P R 1953 *Rev. Mod. Phys.* **25** 269
- [30] Gilmore K, Idzerda Y U, Klem M T, Allen M, Douglas T and Young M 2005 *J. Appl. Phys.* **97** 10B301
- [31] Bodker F, Morup S and Linderroth S 1994 *Phys. Rev. Lett.* **72** 282
- [32] Huber D L and Seehra M S 1975 *J. Phys. Chem. Solids* **36** 723
- [33] Seehra M S and Gupta R P 1974 *Phys. Rev. B* **9** 197
- [34] Birgeneau R J, Rupp L W Jr, Guggenheim H J, Lindgard P A and Huber D L 1972 *Phys. Rev. Lett.* **30** 1252
- [35] Rettori C *et al* 1997 *Phys. Rev. B* **55** 3083
- [36] Rehtin M D and Averbach B L 1972 *Phys. Rev. B* **6** 4294
- [37] Huber D L 1972 *Phys. Rev. B* **6** 3180
Huber D L and Seehra M S 1976 *Phys. Status Solidi b* **74** 145